Strongly correlated photons with quantum feedback in a cascaded nanoscale double-cavity system

Jiahua Li,[1,*] Chunling Ding,[2,†] and Ying Wu[1,‡]

[1]*School of Physics, Huazhong University of Science and Technology, Wuhan 430074, People's Republic of China*

[2]*Hubei Key Laboratory of Optical Information and Pattern Recognition, Wuhan Institute of Technology, Wuhan 430205, People's Republic of China*

(Received 21 June 2020; accepted 8 September 2020; published 6 October 2020)

We characterize via the second-order correlation function the quantum correlations in the transmitted light in a two-cascaded-cavities system side-coupled to a common waveguide via bidirectional propagation. Adopting a full quantum master equation and standard input-output theory, we calculate the zero-time-delay second-order correlation function and identify clearly distinguished parameter regimes with the photon bunching and antibunching. Our numerical results clearly show that strong photon antibunching can be achieved in the cascaded double-cavity system without the need for extra modal-overlap-based coupling between the two cavities. Remarkably, this strong photon antibunching appears in the weak-coupling regime of cavity quantum electrodynamics. The photon antibunching properties can be manipulated by adjusting the propagation phase. In addition, we discuss the influences of the emitter-to-cavity coupling strength and the waveguide-to-cavity coupling rate on the photon antibunching. Also, the experimental feasibility of our proposal with the current photonic crystal technique is analyzed. This study offers an alternative way to generate the strongly antibunched photons, which may have applications in on-chip quantum information processing.

DOI: 10.1103/PhysRevA.102.043701

I. INTRODUCTION

In 1976, two different groups, Kimble and Mandel [1] as well as Carmichael and Walls [2], showed theoretically that the resonance fluorescence of a two-level atom excited by a quantum electromagnetic field can exhibit photon antibunching. One year later, Kimble *et al.* [3] observed the phenomenon of photon antibunching in resonance fluorescence by using sodium atoms. From then on, studies about strongly correlated photons have attracted considerable attention [4,5] due to their potential applications in quantum information technologies [6–9]. Especially, cavity quantum electrodynamics consisting of optical microcavities (e.g., Fabry–Perot cavities, micropillar cavities, microtoroidal cavities, or photonic crystal cavities) strongly coupled to quantum emitters [e.g., atoms, color centers, molecules, or quantum dots (QDs)] in recent years have made great progress, which can yield large optical nonlinearity even at the single-photon level [10–12] and induce an anharmonic Jaynes-Cummings ladder [13–15]. Correspondingly, this gives rise to strong quantum correlation phenomena, including photon antibunching and bunching [16–21]. In the scenario of photon antibunching, coupling of a single photon to the system prohibits the coupling of the subsequent photons (tending to arrive one-by-one). On the contrary, for photon bunching, coupling of initial photons facilitates the coupling of the subsequent photons (tending to arrive in bundles). To generate this convenient photon antibunching, strong nonlinear interaction is one of the necessary prerequisites [22,23]. Alternatively, it has been reported that the photon antibunching phenomena can also be found in circuit quantum electrodynamics systems [24,25], waveguide quantum electrodynamics systems [26,27], cavity optomechanical systems [28–30], nanoplasmonic cavity-emitter systems [31–33], patterned two-dimensional material monolayer-cavity systems [34,35], and other special systems [36–41].

In 2010, a new mechanism named unconventional photon antibunching and based on the destructive quantum interference between multiple transition pathways in two directly coupled cavities (also called photonic molecules) instead of one cavity was proposed theoretically by Liew and Savona [42]. This photonic molecule only requires weak nonlinearities in the cavities or weak interactions with the emitter to create single photons [42,43]. After that, various nonlinear optical systems based on this underlying mechanism were put forward to realize the photon antibunching effect, including two directly coupled single-mode cavities with second-order or third-order optical nonlinearity [44–50], bimodal optical cavity containing a single QD [51–54], coupled cavity optomechanical systems [55–57], and coupled polaritonic systems [58–61], etc., just to name a few examples.

As far as the two cavities are concerned, generally their coupling approach can be categorized into two typical configurations: One "cavity-cavity" configuration is to directly couple two cavities via the modal overlap in the space [44–50]. Other possible "cavity-waveguide-cavity" configurations are to cascade two cavities (without the spatially modal overlap) via a common waveguide, among which there exists (i) purely unidirectional propagation (or scattering) of fields without feedback [62–66] and (ii) bidirectional propagations of fields with feedback [67–70]. We note that the vast majority of the previous studies to date on the unconventional photon antibunching involving two cavities are based on the former,

*huajia_li@163.com
†clding2006@126.com
‡yingwu2@126.com

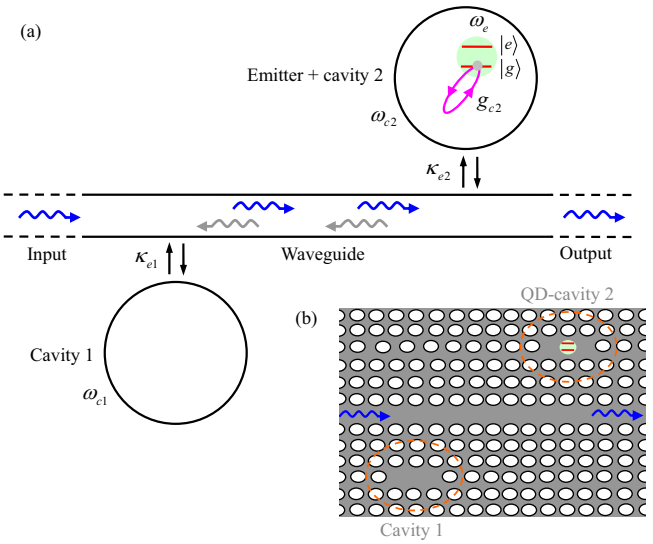

FIG. 1. (a) Sketch of the cascaded setup with feedback under study: A pair of single-mode cavities (labeled 1 and 2), which have no mutual coupling by spatially modal overlap but are side-coupled to a common waveguide representing the input and output ports of our system, and where one of both cavities, i.e., the cavity 2, is coupled to a single two-level emitter with the ground and excited states $|g\rangle$ and $|e\rangle$. The waveguide is bidirectional, which allows the light fields to propagate in the forward and backward directions indicated by the blue and gray wavy arrows. Both cavities are arranged such that the output from cavity 1 is the input of cavity 2 while the output of cavity 2 feeds back into cavity 1 and also are separated by a long enough distance L such that there is no direct coupling between both cavities. In our model, there is only a laser input in the forward direction (blue wavy arrow) and no laser input in the reversal direction. The transmitted field is detected. The involved parameters are defined in more detail in the text. (b) Specific on-chip implementation plan of schematic (a) using planar photonic crystal structure: Two L3-type photonic crystal nanocavities, a line-defect photonic crystal waveguide, and a semiconductor QD embedded in one nanocavity 2. A small light-green shaded circle denotes the position of the QD.

i.e., two directly coupled cavities via the modal overlap. One natural question is whether there exists strongly correlated photon transmission in the latter-two cascaded cavities side-coupled to a common waveguide via (ii) bidirectional propagations of fields with feedback; see Fig. 1. Is it possible to optimize the structure design so that the degree of the photon antibunching can be significantly enhanced even in the weak-coupling regime of cavity quantum electrodynamics where the loss rate exceeds the coherent interaction strength between the emitter and the cavity mode?

In the present work, we give an in-depth investigation addressing these questions. The system under study consists of two single-mode cavities, one of which contains a single two-level quantum emitter and which has no coupling by spatial proximity but is side-coupled to a common bidirectional waveguide. By numerically calculating the zero-time-delay second-order correlation function [71], we can identify clearly distinguished parameter regimes with the photon bunching and antibunching in such a cascaded cavity-waveguide-cavity quantum electrodynamics architecture with quantum feedback. We show that the strong photon antibunching of the transmitted light can be obtained under the proper conditions. The degree of the photon antibunching can be controlled to change periodically by adjusting the propagation phase associated with the distance between the two cavities. The fundamental physics behind this quantum correlation phenomenon is understood. The influences of the other system parameters, including the emitter-to-cavity coupling strength and the waveguide-to-cavity coupling rate, on the antibunching are discussed in detail. What is more, the optimal condition for strong photon antibunching is analyzed. It is revealed that the enhanced photon antibunching originates from destructive interference induced by the bidirectional propagations of light fields belonging to the two cavities. We also discuss the feasibility of the proposed scheme by using current state-of-the-art photonic crystal samples.

On the one hand, unlike Refs. [42–50], here the proposed scheme is not required to maintain high cavity-cavity coupling (i.e., coherent hopping) by the spatial proximity. It should be pointed out that in the nanophotonics platform, this requirement about maintaining both individual addressability and high coupling strength between the two cavities may be challenging in experiment because, in general, the intercavity coupling is obtained by the spatial proximity. On the other hand, our scheme for generating photon antibunching can operate in the weak-coupling regime, in contrast with conventional photon antibunching in the strong-coupling regime in the previous literature [16–20]. So this weak-coupling condition relaxes considerably the requirements on the system parameters, which makes the experimental implementation of this proposal easy. Finally, in our model, the two cavities are arranged such that only a single driving input is applied to cavity 1 and the output of cavity 1 forms the input of cavity 2 via the waveguide channel, which is completely different from the previous schemes adopting two individual inputs to respectively drive the two cavities [44,47–50,52]. As a consequence, the present cascaded cavity-waveguide-cavity quantum electrodynamics is simple for engineering and fabrication in the solid-state QD-photonic-crystal platform, and the way of the achievable photon antibunching is important for the future generation of tunable single-photon-emission sources.

The rest of this paper is organized as follows: In Sec. II we present the physical model and describe the theoretical approach, namely, the full quantum master equation including incoherent processes, for the considered quantum correlation in a cascaded bidirectional cavity-waveguide-cavity quantum electrodynamics architecture. In Sec. III we analyze the experimental feasibility of our proposal based on the solid-state QD and photonic crystal platform. In Sec. IV, we discuss how to calculate the second-order correlation function of the transmitted field. Numerical and analytical results for the characteristics of the second-order photon correlation are collected in Sec. V. The transmission properties of the system are also analyzed. Finally, the paper is summarized in Sec. VI.

II. PHYSICAL SYSTEM AND THEORETICAL FRAMEWORK

The system of interest is depicted schematically in Fig. 1(a), where an empty cavity labeled 1 is driven with an

external pump laser via an input channel and another cavity labeled 2 contains and interacts with a two-level quantum emitter, whose ground and excited states are denoted by $|g\rangle$ and $|e\rangle$, respectively. In the presence of the embedded emitter in cavity 2, the dynamics of the system can become nonlinear. We assume that the output of cavity 1 forms the input of cavity 2 via the common waveguide channel, at the same time the output of cavity 2 also feeds back into cavity 1 (called quantum feedback; see gray wavy arrows in Fig. 1), which we will refer to as a cascaded quantum system with bidirectional propagating information flows [67–70]. Notice that we consider that the two cavities 1 and 2 are separated by a sufficiently long distance L much longer than their wavelengths, so there is no direct modal overlap (i.e., no coupling) between the two cavity modes but, nevertheless, these two cavities are closely connected through this bidirectional waveguide. In the rotating frame of the pump-laser frequency ω_p, the dynamics of our cascaded bidirectional cavity-waveguide-cavity quantum electrodynamics system as shown in Fig. 1(a), including the incoherent processes, follows the master equation according to Refs. [64,70] (we take hereafter $\hbar = 1$):

$$\begin{aligned}\frac{d\hat{\rho}}{dt} &= i[\hat{\rho}, \hat{H}_{\rm sys1} + \hat{H}_{\rm sys2}] \\ &\quad + \gamma_s \mathcal{L}(\hat{\sigma})\hat{\rho} + \gamma_d \mathcal{L}(\hat{\sigma}^\dagger\hat{\sigma})\hat{\rho} \\ &\quad + \kappa_1 \mathcal{L}(\hat{c}_1)\hat{\rho} + \kappa_2 \mathcal{L}(\hat{c}_2)\hat{\rho} \\ &\quad + \sqrt{\kappa_{e1}\kappa_{e2}}(e^{i\phi}[\hat{c}_1, \hat{\rho}\hat{c}_2^\dagger] + e^{i\phi}[\hat{c}_2, \hat{\rho}\hat{c}_1^\dagger] + \text{H.c.}), \end{aligned} \tag{1}$$

with $\hat{\rho}$ being the density-matrix operator of the system, the notation $[\bullet, \bullet]$ being the commutation relation, and H.c. being the Hermitian conjugate.

The Hamiltonians $\hat{H}_{\rm sys1}$ and $\hat{H}_{\rm sys2}$ of the empty cavity 1 and the emitter-coupled cavity 2 within the dipole and rotating-wave approximations read

$$\hat{H}_{\rm sys1} = \Delta_{c1}\hat{c}_1^\dagger\hat{c}_1 + \sqrt{\kappa_{e1}}\left[c_1^{\rm in}\hat{c}_1^\dagger + \left(c_1^{\rm in}\right)^*\hat{c}_1\right], \tag{2}$$

$$\begin{aligned}\hat{H}_{\rm sys2} &= \Delta_{c2}\hat{c}_2^\dagger\hat{c}_2 + (\Delta_{c2} + \Delta_{e2})\hat{\sigma}^\dagger\hat{\sigma} + g_{c2}(\hat{c}_2\hat{\sigma}^\dagger + \hat{c}_2^\dagger\hat{\sigma}) \\ &\quad + \sqrt{\kappa_{e2}}\left[c_1^{\rm in}e^{i\phi}\hat{c}_2^\dagger + \left(c_1^{\rm in}\right)^*e^{-i\phi}\hat{c}_2\right], \end{aligned} \tag{3}$$

where $\hat{c}_1$ ($\hat{c}_1^\dagger$) and $\hat{c}_2$ ($\hat{c}_2^\dagger$) are the photon annihilation (creation) operators for the cavity-1 and -2 modes, respectively; $\hat{\sigma} = |g\rangle\langle e|$ ($\hat{\sigma}^\dagger = |e\rangle\langle g|$) is the electronic lowing (raising) transition operators between states $|g\rangle$ and $|e\rangle$ for the two-level emitter; $c_1^{\rm in}$ is the amplitude of the continuous-wave external input pump laser only in the forward direction, initially which is used to drive the cavity-1 mode at a rate $\sqrt{\kappa_{e1}}$ and can be expressed as $\mathcal{E}_p(t) = c_1^{\rm in}e^{-i\omega_p t}$ with the angular frequency ω_p; $\Delta_{c1} = \omega_{c1} - \omega_p$ is the detuning of the cavity-1 resonance frequency ω_{c1} with respect to the pump laser ω_p; $\Delta_{c2} = \omega_{c2} - \omega_p$ is the detuning of the cavity-2 resonance frequency ω_{c2} with respect to the pump laser ω_p; and $\Delta_{e2} = \omega_e - \omega_{c2}$ is the detuning of the two-level emitter ω_e (the energy of the emitter ground state $|g\rangle$ is set as zero point, i.e., $\omega_g = 0$) with respect to the cavity-2 resonance frequency ω_{c2}. When introducing the detuning $\delta_{21} = \omega_{c2} - \omega_{c1}$ between the two cavities, we have the relationship $\Delta_{c2} = \Delta_{c1} + \delta_{21}$. g_{c2} is the coupling strengths between cavity 2 and the two-level emitter, depending on the electric-dipole moment μ_{eg} of the emitter transition and the mode volume V of the cavity, i.e., $g_{c2} = \mu_{eg}\sqrt{\omega_{c2}/2\hbar\epsilon_0 V}$, with ϵ_0 being the vacuum permittivity. The propagation phase factor ϕ will be explained later on.

The Lindblad superoperator $\mathcal{L}(\hat{\mathcal{O}})$ describes the dissipative coupling to the external baths and takes the form

$$\mathcal{L}(\hat{\mathcal{O}})\hat{\rho} = \tfrac{1}{2}(2\hat{\mathcal{O}}\hat{\rho}\hat{\mathcal{O}}^\dagger - \hat{\mathcal{O}}^\dagger\hat{\mathcal{O}}\hat{\rho} - \hat{\rho}\hat{\mathcal{O}}^\dagger\hat{\mathcal{O}}), \tag{4}$$

for the collapse operator $\hat{\mathcal{O}}$ corresponding to the specific dissipation process. More specifically, the second term on the right-hand side (RHS) of Eq. (1) corresponds to the two-level emitter damping, where γ_s is the spontaneous emission decay rate of the emitter. The third term represents the pure dephasing of the emitter, where γ_d is the pure dephasing rate of the emitter. Note that, for gaseous-state emitters such as atoms and ions, we neglect dephasing effects because the pure dephasing rate γ_d is much smaller than the spontaneous emission decay rate γ_s. However, for solid-state emitters such as QDs, the pure dephasing rate γ_d becomes relevant, which is much larger than the spontaneous emission decay rate γ_s. The fourth and fifth terms on the RHS of Eq. (1) stand for the cavity-1 and -2 dampings, where κ_1 and κ_2 are the total loss rates (or cavity linewidths) of the two cavities. κ_1 is the sum of the intrinsic (κ_{i1}) and extrinsic (κ_{e1}) loss rates, i.e., $\kappa_1 = \kappa_{i1} + 2\kappa_{e1}$ for the cavity-1 mode. Likewise, $\kappa_2 = \kappa_{i2} + 2\kappa_{e2}$ for the cavity-2 mode. The former (κ_{i1}, κ_{i2}) is due to loss in the cavity modes themselves, whereas the latter ($2\kappa_{e1}, 2\kappa_{e2}$) is due to the coupling of the cavity modes to the waveguide from the forward and backward directions. For notational simplicity, we have assumed them to be the same for both directions.

Finally, the sixth term on the RHS of Eq. (1) describes forward-backward bidirectional scattering, or two-way information flows: The output from cavity 1 is the input of cavity 2, simultaneously the output of cavity 2 feeds back into cavity 1 [70]. Physically, this term models the dissipative coupling at the rate $\sqrt{\kappa_{e1}\kappa_{e2}}$. The factor ϕ is the photon propagation phase [67–70] when the input pump laser propagates from cavity 1 to cavity 2 or vice versa and is expressed by $\phi = \beta(\omega)L$, where $\beta(\omega)$ is the waveguide's dispersion and L denotes the center distance between the two cavities. Obviously, the propagation phase ϕ can be tuned by appropriately changing the distance L between the two cavities. On the other hand, the dispersion $\beta(\omega)$ of the waveguide can also be used to control the propagation phase ϕ. This propagation phase ϕ is of interest to us, since it determines the photon correlation (cf. discussion below).

III. DISCUSSION OF THE EXPERIMENTAL IMPLEMENTATION OF THE MODEL

Now we address the experiment feasibility of the proposed scheme. Ultrahigh-Q photonic crystal nanocavities have been realized in a two-dimensional triangular-lattice air-hole photonic crystal slab [72–74], which is a promising platform for the experimental implementation of our model; see Fig. 1(b) for a sketch of our setup (not to scale). The photonic crystal structures can be fabricated by using electron-beam lithography, followed by inductively coupled plasma dry etching and selective wet etching of the sacrificial AlGaAs layer. The linear defects are introduced to form two L3-type photonic-crystal nanocavities, where "3″ denotes the number of missing

air holes. To further improve the cavity quality factor Q, the holes adjacent to the cavity need to be shifted properly. A line-defect W1-type photonic-crystal waveguide is formed by missing a row of holes in between the two nanocavities and separated from them by three rows of holes. Coupling efficiency, i.e., the ratio of light leaking from cavity mode into the waveguide to the total leakage, can be controlled by the gap between the cavity and waveguide. The two nanocavities are directly side-coupled to a common photonic crystal waveguide along the ΓK lattice direction, but have no direct coupling owing to the three-row spacing and sufficiently long separation distance $L \approx 12a$, a being the lattice constant of the underlying photonic crystal lattice, according to the experimental data of Refs. [75,76]. The distance L between the two cavities can be adjusted by changing the number of periods. The detailed characterization of similar structures and the fabrication process are described elsewhere [75,76].

For the above-mentioned two-level emitter confined in one of the two L3 photonic crystal nanocavities, we can adopt a low-density self-assembled InGaAs/InAs QD because of its large dipole moment [77] and good integration [78]. Semiconductor QDs can be grown by molecular-beam epitaxy [79], where the simple two-level approximation is valid for small epitaxial QD. A single QD can be added to the L3 nanocavity based on precise positioning techniques of atomic force microscopy [80]. In the experiment, the strong couplings between the L3 photonic crystal nanocavity and the QD have been observed [81,82]. Experimental results [83–85] have shown that the QD transition can be tuned through the cavity resonance by using the local-temperature-tuning technique.

The parameters of the coupled photonic crystal waveguide, L3 nanocavity, and QD system used in the calculations are adopted according to the existing experimental data of Refs. [86–90]. By improving the spatial alignment of the QD and cavity field, the coupling strength can reach values up to $g_c/2\pi \approx 40$ GHz as reported in Ref. [91]. Hence, within experimentally achievable parameter ranges we choose $g_{c2}/2\pi = 15$ GHz [86,87]. In particular, recent improvements in design and fabrication have allowed for intrinsic loss rates as low as $\kappa_i/2\pi \approx 4$ GHz in experimental GaAs photonic crystal nanocavity [92]. Here we assume that each nanocavity has the same modest intrinsic loss rate; that is, $\kappa_{i1}/2\pi = \kappa_{i2}/2\pi = 15$ GHz [89]. The extrinsic loss rates κ_{e1} and κ_{e2} depend on the distance between the photonic crystal waveguide and nanocavity, which can be postfabrication tailored by carefully dimensioning the structure. As an example, here $\kappa_{e1}/2\pi = \kappa_{e2}/2\pi = 10$ GHz are considered for the two L3 nanocavities side-coupled to the waveguide, which are readily available in experiments [82]. With these given parameter values above, the loaded (including the waveguide coupling) and intrinsic quality factors are estimated to be 5500 and 13 000 at the cavity resonance wavelength $\lambda_{c1} = \lambda_{c2} = 1550$ nm (telecom band). Thanks to the total loss rate of the system being much larger than the QD-cavity coupling strength, i.e., $\kappa_2 > g_{c2}$, the QD-cavity system operates in the weak-coupling regime (also called the bad-cavity limit). Following Refs. [87,90], we set the spontaneous emission decay rate and the pure dephasing rate for solid-state QD to be $\gamma_s/2\pi = 0.16$ GHz and $\gamma_d/2\pi = 1$ GHz, respectively.

Finally, coupling to the photonic crystal waveguide can be obtained through microscope objectives and micropositioners [93]. The photon correlation of the transmitted signal is measured experimentally by using a Hanbury-Brown and Twiss device, which comprises one fiber beam splitter and a pair of single-photon avalanche photodiodes [94,95].

IV. CALCULATION OF SECOND-ORDER PHOTON CORRELATION $g^{(2)}(0)$

Here, we discuss how to calculate the second-order correlation function $g^{(2)}(0)$ of the transmitted field. In the present study, we are interested in the statistical properties of the transmitted photons from the waveguide channel in this cascaded cavity-waveguide-cavity quantum electrodynamics system (see Fig. 1). Following the input-output theory from quantum optics [62–64], we can achieve the transmission amplitude $\hat{c}_2^{\rm out}$ of the system, with the form

$$\hat{c}_2^{\rm out} = e^{i\phi}\left(c_1^{\rm in} - i\sqrt{\kappa_{e1}}\hat{c}_1\right) - i\sqrt{\kappa_{e2}}\hat{c}_2, \tag{5}$$

and then the statistical properties of the transmitted photons can be described by the normalized zero-time-delay second-order correlation function [71]

$$g^{(2)}(0) = \frac{\left\langle \left(\hat{c}_2^{\rm out\dagger}\right)^2 \left(\hat{c}_2^{\rm out}\right)^2 \right\rangle}{\left\langle \hat{c}_2^{\rm out\dagger}\hat{c}_2^{\rm out}\right\rangle^2}, \tag{6}$$

which characterizes the joint probability of detecting two photons at the same time. The symbol $\langle\bullet\rangle$ denotes the quantum expectation value. From the density matrix the expectation value of an observable $\hat{\mathcal{A}}$ can be computed as $\langle\hat{\mathcal{A}}\rangle = {\rm Tr}(\hat{\mathcal{A}}\hat{\rho})$, where Tr denotes the trace. When the condition $g^{(2)}(0) < 1$ holds, the sub-Poisson statistics of the transmission field appears, which is a nonclassical effect often called photon antibunching. In contrast, the condition of $g^{(2)}(0) > 1$ corresponds to super-Poisson statistics, which is a classical effect referred to as photon bunching for $2 > g^{(2)}(0) > 1$ and photon superbunching for $g^{(2)}(0) > 2$. In particular, the value of $g^{(2)}(0) = 1$ corresponds to a Poissonian distribution typical of coherent light and $g^{(2)}(0) = 2$ corresponds to thermal or chaotic light. Hence we can determine whether the antibunching happens according to $g^{(2)}(0)$.

On the other hand, according to Eq. (5), the corresponding normalized transmission intensity is yielded by $T = \langle\hat{c}_2^{\rm out\dagger}\hat{c}_2^{\rm out}\rangle/(c_1^{\rm in})^2$. In what follows, we will calculate the second-order correlation function $g^{(2)}(0)$ and the transmission T of the system by numerically solving the master equation (1) within a truncated Hilbert space under the steady state (i.e., setting $d\hat{\rho}/dt = 0$, which is independent of the initial states). The numerical results are presented in Figs. 2–7 below in various parameter spaces.

V. NUMERICAL RESULTS AND DISCUSSIONS ABOUT CORRELATION $g^{(2)}(0)$ TOGETHER WITH TRANSMISSION T

First of all, let us focus on how the propagation phase ϕ modifies quantum correlations between photons. In Fig. 2, we plot the zero-delay second-order correlation function $g^{(2)}(0)$ of the transmitted field as a function of the detuning $\Delta_{c1}/2\pi$

with the four different values of the propagation phase ϕ. As shown in the figure, the photon correction of the output light depends so sensitively on the propagation phase ϕ that the corresponding profiles of $g^{(2)}(0)$ are quite different. Specifically, for the scenario that $\phi = m\pi$ with m being an integer in Fig. 2(a), the spectrum of the second-order correlation function $g^{(2)}(0)$ is symmetric with respect to the resonance point $\Delta_{c1}/2\pi = 0$ GHz, which exhibits the two bunching peaks between the three antibunching dips. Here, for the sake of convenience we term the corresponding antibunching dips (bunching peaks) as the left-sideband, central, and right-sideband ones (the left-sideband and right-sideband ones) from left to right in all the figures. For the central antibunching dip at $\Delta_{c1}/2\pi = 0$ GHz, the value of $g^{(2)}(0)$ reaches $g^{(2)}(0) \simeq 0.84$. For the left-sideband and right-sideband antibunching dips at $\Delta_{c1}/2\pi = \pm 19$ GHz, the depth of the two antibunching dips becomes shallow obviously with respect to the central antibunching dip, where we have the values $g^{(2)}(0) \simeq 0.91$. On the other hand, for the left-sideband and right-sideband bunching peaks at $\Delta_{c1}/2\pi = \pm 13$ GHz, the values of $g^{(2)}(0)$ arrive at $g^{(2)}(0) \simeq 1.7$.

Whereas when $\phi = m\pi + \pi/4$ in Fig. 2(b), the correlation spectrum of $g^{(2)}(0)$ evolves into an asymmetric profile with respect to $\Delta_{c1}/2\pi = 0$ GHz. It can be seen that the central antibunching dip moves with and shifts slightly toward the right direction, with a minimum value of $g^{(2)}(0) \simeq 0.25$ at $\Delta_{c1}/2\pi = 3$ GHz. The depth of the left-sideband and right-sideband antibunching dips increases and reaches the values $g^{(2)}(0) \simeq 0.71$ at $\Delta_{c1}/2\pi = -16$ GHz and $g^{(2)}(0) \simeq 0.81$ at $\Delta_{c1}/2\pi = 19$ GHz, respectively. The height of the left-sideband bunching peak increases slightly with a value of $g^{(2)}(0) \simeq 1.8$ at $\Delta_{c1}/2\pi = -11$ GHz. However, the height of the right-sideband bunching peak increases significantly, with a maximum value of $g^{(2)}(0) \simeq 3.1$ at $\Delta_{c1}/2\pi = 13$ GHz, which shows superbunching because of $g^{(2)}(0) > 2$.

For the case that $\phi = m\pi + \pi/2$ in Fig. 2(c), although the spectral structure of $g^{(2)}(0)$ is similar to that for the case that $\phi = m\pi$ in Fig. 2(a), the degree of the photon bunching and antibunching is enhanced obviously. Most strikingly, the depth of the central antibunching dip at $\Delta_{c1}/2\pi = 0$ GHz increases considerably and reaches a value as low as $g^{(2)}(0) \simeq 0.07$ much smaller than for either $\min\{g^{(2)}(0)\} \simeq 0.84$ in Fig. 2(a), or $\min\{g^{(2)}(0)\} \simeq 0.25$ in Fig. 2(b). Likewise, for the left-sideband and right-sideband antibunching dips at $\Delta_{c1}/2\pi = \pm 17$ GHz, the value of $g^{(2)}(0)$ also decreases and reaches $g^{(2)}(0) \simeq 0.65$. Nevertheless, for the left-sideband and right-sideband bunching peaks at $\Delta_{c1}/2\pi = \pm 12$ GHz, the value of $g^{(2)}(0)$ rapidly increases and reaches $g^{(2)}(0) \simeq 3.4$, which displays superbunching $[g^{(2)}(0) > 2]$.

With a further increase in ϕ, e.g., $\phi = m\pi + 3\pi/4$ in Fig. 2(d), the spectrum of $g^{(2)}(0)$ again becomes asymmetric with respect to the spectrum center. The minimum for $g^{(2)}(0)$ occurs at $\Delta_{c1}/2\pi = -3$ GHz, which corresponds to the central antibunching dip and yields a value of $g^{(2)}(0) \simeq 0.25$. The left-sideband antibunching dip for $g^{(2)}(0)$ yields a value of $g^{(2)}(0) \simeq 0.81$ at $\Delta_{c1}/2\pi = -19$ GHz and the right-sideband antibunching dip yields a value of $g^{(2)}(0) \simeq 0.71$ at $\Delta_{c1}/2\pi = 16$ GHz. The left-sideband bunching peak reaches a maximum at $\Delta_{c1}/2\pi = -13$ GHz with a value $g^{(2)}(0) \simeq 3.1$. The right-sideband bunching peak for $g^{(2)}(0)$

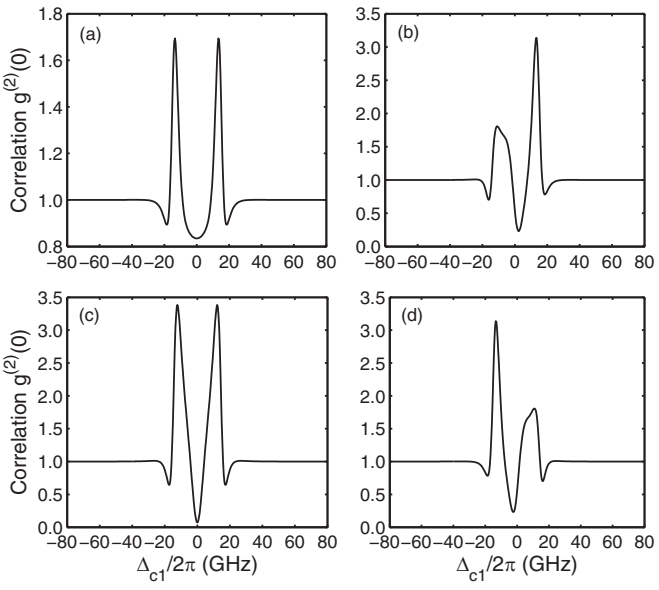

FIG. 2. The second-order correlation function $g^{(2)}(0)$ versus the detuning $\Delta_{c1}/2\pi$ for four different values of the propagation phase factor ϕ: (a) $\phi = m\pi$, (b) $\phi = m\pi + \pi/4$, (c) $\phi = m\pi + \pi/2$, and (d) $\phi = m\pi + 3\pi/4$ (m is an integer). The other parameters of the system are chosen as $g_{c2}/2\pi = 15$ GHz, $\kappa_{i1}/2\pi = \kappa_{i2}/2\pi = 15$ GHz, $\kappa_{e1}/2\pi = \kappa_{e2}/2\pi = 10$ GHz, $\gamma_s/2\pi = 0.16$ GHz, $\gamma_d/2\pi = 1$ GHz, $\delta_{21}/2\pi = 0$ GHz, $\Delta_{e2}/2\pi = 0$ GHz, and $c_1^{\rm in}\sqrt{\kappa_{e1}}/2\pi = 1$ GHz.

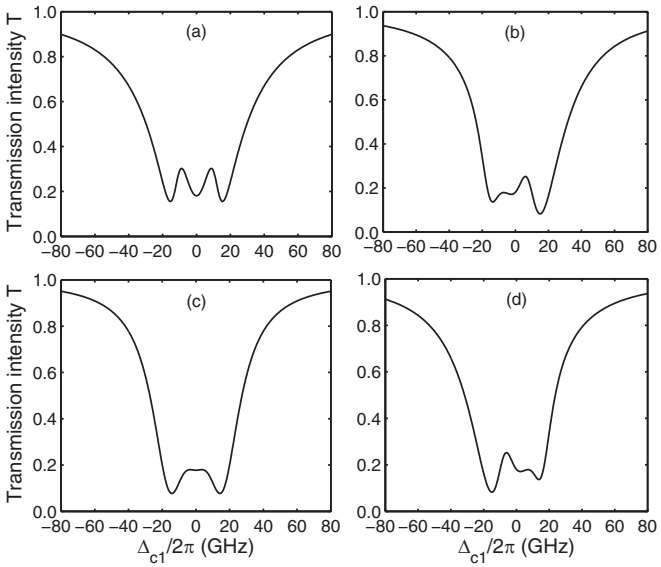

FIG. 3. The normalized transmission intensity T as a function of the detuning $\Delta_{c1}/2\pi$ for four different values of the propagation phase factor ϕ: (a) $\phi = m\pi$, (b) $\phi = m\pi + \pi/4$, (c) $\phi = m\pi + \pi/2$, and (d) $\phi = m\pi + 3\pi/4$ (m is an integer). The other parameters of the system are chosen as $g_{c2}/2\pi = 15$ GHz, $\kappa_{i1}/2\pi = \kappa_{i2}/2\pi = 15$ GHz, $\kappa_{e1}/2\pi = \kappa_{e2}/2\pi = 10$ GHz, $\gamma_s/2\pi = 0.16$ GHz, $\gamma_d/2\pi = 1$ GHz, $\delta_{21}/2\pi = 0$ GHz, $\Delta_{e2}/2\pi = 0$ GHz, and $c_1^{\rm in}\sqrt{\kappa_{e1}}/2\pi = 1$ GHz.

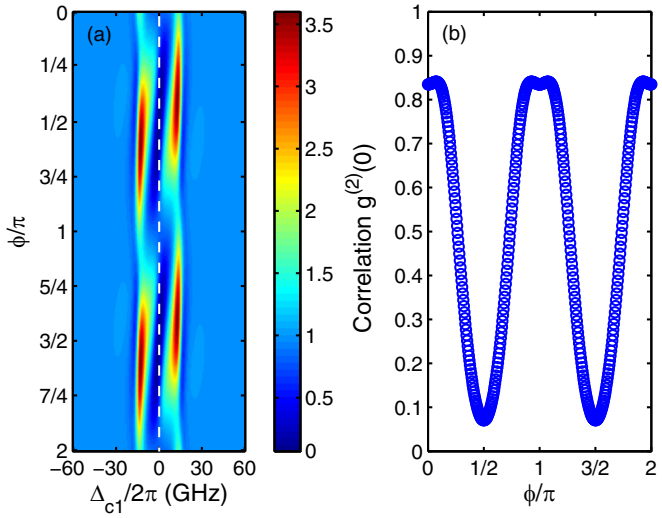

FIG. 4. (a) Two-dimensional plot of the second-order correlation function $g^{(2)}(0)$ as a function of the detuning $\Delta_{c1}/2\pi$ and the propagation phase factor ϕ. The color bar corresponds to the values of $g^{(2)}(0)$. (b) A cut through the left-hand panel (a) along the indicated vertical white dashed line, i.e., $\Delta_{c1}/2\pi = 0$ GHz. The other parameters of the system are chosen as $g_{c2}/2\pi = 15$ GHz, $\kappa_{i1}/2\pi = \kappa_{i2}/2\pi = 15$ GHz, $\kappa_{e1}/2\pi = \kappa_{e2}/2\pi = 10$ GHz, $\gamma_s/2\pi = 0.16$ GHz, $\gamma_d/2\pi = 1$ GHz, $\delta_{21}/2\pi = 0$ GHz, $\Delta_{e2}/2\pi = 0$ GHz, and $c_1^{\rm in}\sqrt{\kappa_{e1}}/2\pi = 1$ GHz.

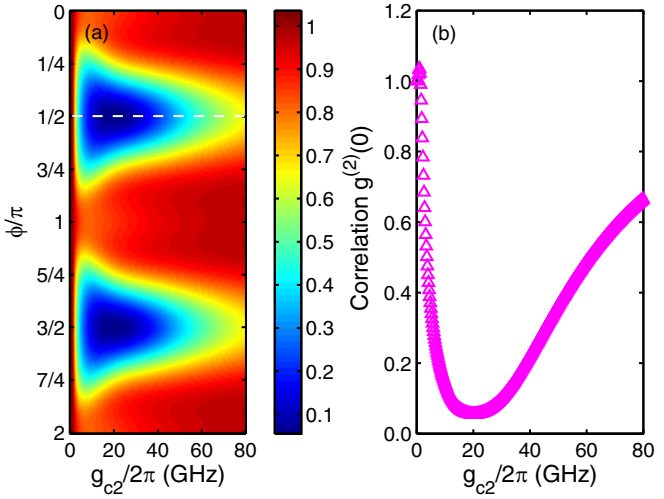

FIG. 6. (a) Two-dimensional plot of the second-order correlation function $g^{(2)}(0)$ as a function of the QD-cavity coupling strength $g_{c2}/2\pi$ and the propagation phase factor ϕ. The color bar represents the values of $g^{(2)}(0)$. (b) A cut through the left-hand panel (a) along the indicated horizontal white dashed line. The other parameters of the system are chosen as $\kappa_{i1}/2\pi = \kappa_{i2}/2\pi = 15$ GHz, $\kappa_{e1}/2\pi = \kappa_{e2}/2\pi = 10$ GHz, $\gamma_s/2\pi = 0.16$ GHz, $\gamma_d/2\pi = 1$ GHz, $\Delta_{c1} = 0$ GHz, $\delta_{21}/2\pi = 0$ GHz, $\Delta_{e2}/2\pi = 0$ GHz, and $c_1^{\rm in}\sqrt{\kappa_{e1}}/2\pi = 1$ GHz.

gives a value of $g^{(2)}(0) \simeq 1.8$ at $\Delta_{c1}/2\pi = 11$ GHz. Comparing Fig. 2(d) with Fig. 2(b), it is evident that the spectrum of $g^{(2)}(0)$ when $\phi = m\pi + 3\pi/4$ in Fig. 2(d) is the mirror image of the spectrum when $\phi = m\pi + \pi/4$ in Fig. 2(b) with respect to $\Delta_{c1}/2\pi = 0$ GHz.

Figures 3(a)–3(d) provide the plots of the normalized transmission intensity T as a function of the detuning $\Delta_{c1}/2\pi$ through the waveguide corresponding to the driving laser utilized in Figs. 2(a)–2(d). Specifically, for the case of $\phi = m\pi$ in Fig. 3(a), we find a symmetric M-type spectral structure with three transmission dips and two transmission peaks,

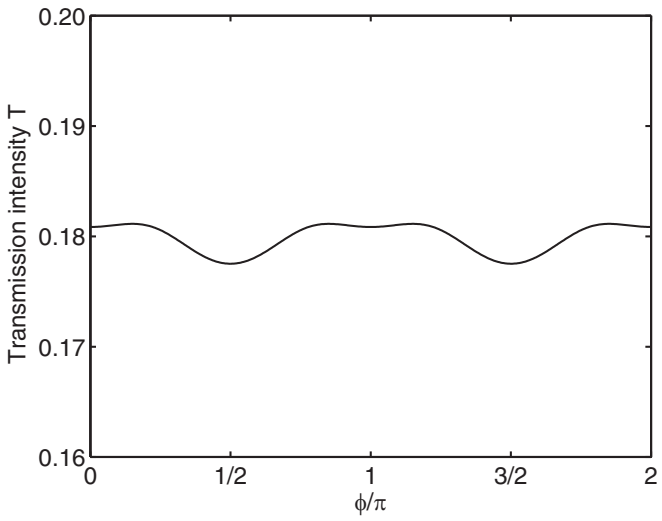

FIG. 5. The normalized transmission intensity T as a function of the propagation phase factor ϕ when $\Delta_{c1}/2\pi = 0$ GHz. The other parameters of the system are chosen as $g_{c2}/2\pi = 15$ GHz, $\kappa_{i1}/2\pi = \kappa_{i2}/2\pi = 15$ GHz, $\kappa_{e1}/2\pi = \kappa_{e2}/2\pi = 10$ GHz, $\gamma_s/2\pi = 0.16$ GHz, $\gamma_d/2\pi = 1$ GHz, $\delta_{21}/2\pi = 0$ GHz, $\Delta_{e2}/2\pi = 0$ GHz, and $c_1^{\rm in}\sqrt{\kappa_{e1}}/2\pi = 1$ GHz.

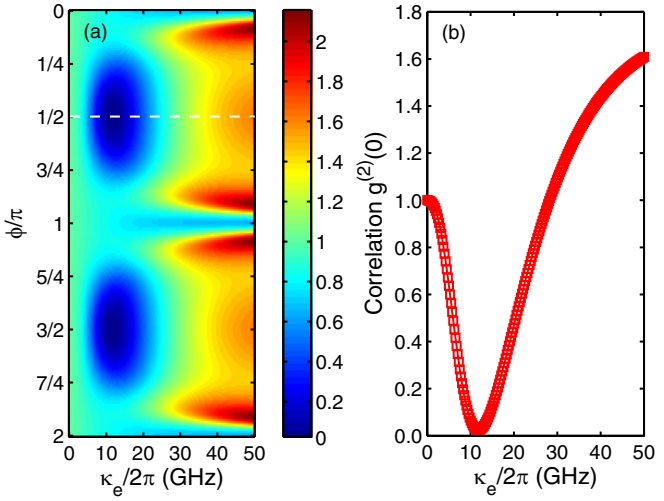

FIG. 7. (a) Two-dimensional plot of the second-order correlation function $g^{(2)}(0)$ as a function of the waveguide-cavity coupling strength $\kappa_e/2\pi$ and the propagation phase factor ϕ. The color bar denotes the values of $g^{(2)}(0)$. (b) A cut through the left-hand panel (a) along the indicated horizontal white dashed line. For convenience, we take $\kappa_{e1} = \kappa_{e2} = \kappa_e$ for both cavities. The other parameters of the system are chosen as $g_{c2}/2\pi = 15$ GHz, $\kappa_{i1}/2\pi = \kappa_{i2}/2\pi = 15$ GHz, $\gamma_s/2\pi = 0.16$ GHz, $\gamma_d/2\pi = 1$ GHz, $\Delta_{c1}/2\pi = 0$ GHz, $\delta_{21}/2\pi = 0$ GHz, $\Delta_{e2}/2\pi = 0$ GHz, and $c_1^{\rm in}/2\pi = 0.2\sqrt{\rm GHz}$.

which is inbuilt in a broad transmission dip. Looking closer, we see that the aforementioned three transmission dips and two transmission peaks just correspond to the three antibunching correlation dips and two bunching correlation peaks of $g^{(2)}(0)$ in Fig. 2(a). For the central antibunching dip at $\Delta_{c1}/2\pi = 0$ GHz, the intensity transmission T arrives at 18.1%. However, when ϕ is tuned to $\phi = m\pi + \pi/4$ in Fig. 3(b), the transmission spectrum of T evolves into an asymmetric lineshape with respect to $\Delta_{c1}/2\pi = 0$ GHz. When $\phi = m\pi + \pi/2$ in Fig. 3(c), the transmission spectrum of T returns to a symmetric profile with two dips and a nearly flat peak lying in the vicinity of the resonance point $\Delta_{c1}/2\pi =$ 0 GHz. As clearly shown, for the situation that the most strong antibunching is generated at $\Delta_{c1}/2\pi = 0$ GHz in Fig. 2(c), the normalized intensity transmission of the system reaches the magnitude of 17.8%. When $\phi = m\pi + 3\pi/4$ in Fig. 3(d), the asymmetric spectrum of T exhibits a mirror image of the spectrum for $\phi = m\pi + \pi/4$ in Fig. 3(b).

For further insight into the above behavior of the photon correlations, we plot the color-scale two-dimensional (2D) map of $g^{(2)}(0)$ as a function of the detuning $\Delta_{c1}/2\pi$ and the propagation phase ϕ in Fig. 4(a), where the color bar represents the magnitude of $g^{(2)}(0)$. As can be seen in Fig. 4(a), on the one hand, $g^{(2)}(0)$ is π periodic with respect to the propagation phase ϕ. As a consequence, any two generating spectra of $g^{(2)}(0)$ at $\phi = X_1$ (X_1 is an arbitrary angle from 0 to π) and $\phi = \pi + X_1$ are exactly identical, as shown in Fig. 4(a). Denoting $g^{(2)}(0)$ with $g^{(2)}(0)[\Delta_{c1}, \phi]$ here, we have an explicit relationship $g^{(2)}(0)[\Delta_{c1}, \phi = X_1] = g^{(2)}(0)[\Delta_{c1}, \phi = \pi + X_1]$. On the other hand, the spectra of $g^{(2)}(0)$ at $\phi = X_2$ (X_2 is an arbitrary angle from 0 to π) and $\phi = \pi - X_2$ are horizontal mirror symmetric, namely, $g^{(2)}(0)[\Delta_{c1}, \phi = X_2] = g^{(2)}(0)[-\Delta_{c1}, \phi = \pi - X_2]$. It should be pointed out that we have carried out extensive numerical calculations (not shown here), all the results support these claims, but it is very difficult to prove the latter claim analytically. The former claim about π periodicity will be explicitly clarified below.

Figure 4(b) shows the cross sections of Fig. 4(a) for the specific value of the detuning $\Delta_{c1}/2\pi = 0$ GHz corresponding to the vertical white dashed line. One can find from Fig. 4(b) that $g^{(2)}(0)$ is less 1 (i.e., antibunching) at $\Delta_{c1}/2\pi =$ 0 GHz for any values of the propagation phase ϕ. Again, it is clearly shown that $g^{(2)}(0)$ varies periodically with varying ϕ, and the period is π. As the propagation phase ϕ is optimized by changing the number of lattice periods, for example taking $\phi = m\pi + \pi/2$, the photon antibunching effect is the strongest as shown in Fig. 4(b). From what has been analyzed above, we can conclude that the degree of the photon antibunching for the transmitted light can be significantly improved and enhanced by adjusting the propagation phase ϕ appropriately.

To get more insights, the normalized transmission intensity T versus the propagation phase ϕ is displayed in Fig. 5. It is shown that, when the optimized phases to collect strong antibunching transmission light are taken as $\phi = m\pi + \pi/2$ (m is an integer, for example, $\phi = \pi/2$ and $\phi = 3\pi/2$), the normalized intensity transmission can reach approximately 17.8% at these phases. The subject of how both the large intensity transmission and the strong photon antibunching of the system are simultaneously achieved can be interesting for straightforwardly measuring such correlations in practical experiments, which is left for further study.

To gain a deeper understanding of the physics behind the above quantum correlation behavior, we begin by rewriting the sixth term in the previous quantum master equation (1) as $\hat{Q}_{\rm st} = \sqrt{\kappa_{e1}\kappa_{e2}}(e^{i\phi}[\hat{c}_1, \hat{\rho}\hat{c}_2^\dagger] + Pe^{i\phi}[\hat{c}_2, \hat{\rho}\hat{c}_1^\dagger] + \text{H.c.})$ by introducing an auxiliary factor P with $P = 0$ or 1. If $P = 0$, the output of cavity 1 drives cavity 2, but there is no backward scattering from cavity 2 to cavity 1, i.e., unidirectional scattering without feedback. In this scenario, Eq. (1) simplifies to the master equation of a cascaded unidirectional quantum system. On the contrary, if $P = 1$, not only the output of cavity 1 drives cavity 2 (forward scattering), but also there is the backward scattering from cavity 2 to cavity 1, i.e., bidirectional scattering with feedback; see Fig. 1. What is more, there is a quantum interference between the forward- and backward-scattering contributions for $P = 1$. When we define $\hat{\tilde{c}}_2 = e^{-i\phi}\hat{c}_2$ and $|\tilde{e}\rangle = e^{i\phi}|e\rangle$ in Eq. (1) as well as $\hat{\tilde{c}}_2^{\rm out} = e^{-i\phi}\hat{c}_2^{\rm out}$ in Eq. (5) together with their Hermitian conjugate, after some algebra, the forms of all the expressions involved in the master equation are kept unchanged except that the sixth term $\hat{Q}_{\rm st} = \sqrt{\kappa_{e1}\kappa_{e2}}(e^{i\phi}[\hat{c}_1, \hat{\rho}\hat{c}_2^\dagger] + Pe^{i\phi}[\hat{c}_2, \hat{\rho}\hat{c}_1^\dagger] + \text{H.c.})$ needs to be changed to

$$\hat{\tilde{Q}}_{\rm st} = \sqrt{\kappa_{e1}\kappa_{e2}}([\hat{c}_1, \hat{\rho}\hat{\tilde{c}}_2^\dagger] + P\underline{e^{2i\phi}}[\hat{\tilde{c}}_2, \hat{\rho}\hat{c}_1^\dagger] + \text{H.c.}). \quad (7)$$

That is to say, after we replace $e^{-i\phi}\hat{c}_2 \to \hat{c}_2$, $e^{i\phi}|e\rangle \to |e\rangle$, $e^{-i\phi}\hat{c}_2^{\rm out} \to \hat{c}_2^{\rm out}$, and $\hat{Q}_{\rm st} \to \hat{\tilde{Q}}_{\rm st}$ throughout, the feature of the system is the same as before the transformation. From Eq. (7), it is quite straightforward to see the following three key points. First, the physical quantities of the system, including but not limited to $g^{(2)}(0)$, are of π periodicity [see the underlined part in Eq. (7)]. Second, the phase dependence of the system would vanish provided that no backward scattering from cavity 2 to cavity 1 exists ($P = 0$ without feedback). So the backward scattering (the feedback) from cavity 2 to cavity 1 plays an important role in controlling $g^{(2)}(0)$. Third, the strong photon antibunching can occur at $\phi = m\pi + \pi/2$ (corresponding to $e^{2i\phi} = -1$) because the destructive interference (corresponding to the minus sign) between the forward- and backward-scattering contributions prevents the escape of photons from the system. These results are consistent with those obtained from Figs. 2 and 4.

Next, it is also interesting to look at the dependency of the second-order correlation function $g^{(2)}(0)$ on the coupling strength $g_{c2}/2\pi$ between the QD and cavity 2. Figure 6(a) shows the color-scale 2D map of $g^{(2)}(0)$ versus the QD-cavity-2 coupling strength $g_{c2}/2\pi$ and the propagation phase ϕ/π. It is seen from Fig. 6(a) that the spectral profile of $g^{(2)}(0)$ is modified dynamically with the changes of both g_{c2} and ϕ. $g^{(2)}(0)$ always varies periodically with varying ϕ, the period is π, but the concrete varying shape is closely associated with the value of g_{c2}. To show this explicitly, by fixing the propagation phase $\phi = \pi/2$ corresponding to the horizontal white dashed line in Fig. 6(a), $g^{(2)}(0)$ versus $g_{c2}/2\pi$ is plotted in Fig. 6(b). As displayed in Fig. 6(b), when QD is inactive (no QD-cavity coupling), i.e., $g_{c2}/2\pi = 0$ GHz, we find that the value of $g^{(2)}(0)$ equals unity. In this situation, the transmitted field is a typically coherent source [$g^{(2)}(0) = 1$]. The reason

for this is that the nonlinearity used to generate photon antibunching is absent in the system with $g_{c2}/2\pi = 0$ GHz. As the coupling strength g_{c2} increases, the value of $g^{(2)}(0)$ decreases rapidly because the strength of the QD-induced nonlinearity increases. After this, $g^{(2)}(0)$ reaches the minimum at the optimal point $g_{c2}^{(\mathrm{opt})} = 2\pi \times 20$ GHz, producing an extremely strong antibunching [$g^{(2)}(0) \simeq 0.05$]. Further increase of g_{c2} above the optimal point $g_{c2}^{(\mathrm{opt})}$ leads to a rise of $g^{(2)}(0)$ and eventually photon bunching because the nonlinearity of the system is saturated and then weakened. As can be also seen in Fig. 6(b), the optimal point $g_{c2}^{(\mathrm{opt})}$ to achieve strong antibunching falls in the weak-coupling regime, i.e., $g_{c2}^{(\mathrm{opt})} < \kappa_2$; this make the experimental realization of the scheme easier.

Finally, we illustrate how the waveguide-cavity coupling strength κ_e affects the second-order correlation function $g^{(2)}(0)$. For notational convenience and without losing generality, here we have set $\kappa_{1e} = \kappa_{2e} = \kappa_e$ for the two cavities. In Fig. 7(a), we plot the color-scale 2D map of $g^{(2)}(0)$ as a function of the waveguide-cavity coupling strength $\kappa_e/2\pi$ and the propagation phase ϕ/π. Figure 7(b) shows the cross sections of Fig. 7(a) for the specific value of the propagation phase $\phi = \pi/2$ corresponding to the horizontal white dashed line. One can find from Fig. 7(a) that the value of $g^{(2)}(0)$ varies periodically upon changing ϕ from 0 to 2π and the corresponding period is π. However, the concrete varying rule of the $g^{(2)}(0)$ profile is directly related to the value of κ_e. For instance, for the case of $\phi = \pi/2$ presented in Fig. 7(b), it can be seen that initially the value of $g^{(2)}(0)$ decreases fast from $g^{(2)}(0) = 1$ upon increasing the coupling strength κ_e and reaches the minimum, i.e., $\min\{g^{(2)}(0)\} \simeq 0.02$ around $\kappa_e^{(\mathrm{opt})}/2\pi \simeq 12$ GHz. With the increase of κ_e above the optimal value $\kappa_e^{(\mathrm{opt})}$, the value of $g^{(2)}(0)$ again grows quickly such that $g^{(2)}(0) > 1$ (bunching). Physically, this behavior is mainly due to the presence of the additional $\hat{Q}_{\mathrm{st}}$ term being $P = 1$ (quantum feedback).

VI. CONCLUSIONS

In summary, we have explored the two-photon correlation characteristics of the transmitted light in a cascaded cavity-waveguide-cavity quantum electrodynamics system with the bidirectional scattering. The considered system is based on the solid-state QD-photonic-crystal platform well within the reach of current experimental abilities and only requires a single drive instead of two individual drives utilized in the previous schemes [44,47–50,52]. By means of the second-order correlation function $g^{(2)}(0)$ and numerical simulations, we can identify clearly distinguished optimal parameter regimes with photon bunching and antibunching. We find that the strong photon antibunching can be obtained in such a cascaded scheme, which, on the one hand, works in the weak-coupling regime and, on the other hand, does not need the intercavity coupling by the spatial proximity compared with the previous systems [42–50]. It is revealed that the photon antibunching properties can be manipulated to change periodically by adjusting the propagation phase appropriately, which is closely associated with the center distance between the two cavities. The fundamental physics behind this quantum correlation phenomenon is presented in support of this statement. Furthermore, we discuss in detail the influence of the QD-to-cavity coupling strength and the waveguide-to-cavity coupling rate on the photon antibunching. Our work provides insights into how to manipulate the second-order correlation function $g^{(2)}(0)$ in such devices. This scheme is compatible with integrated photonics and may have potential application in on-chip quantum information processing. We believe that our proposal is feasible for experimental implementations and deserves to be tested with currently existing technologies.

ACKNOWLEDGMENTS

The help of the anonymous referees in improving this paper is gratefully acknowledged. We also acknowledge the helpful and insightful discussions with Rong Yu, Qu Ye, and Shuting Shen during the paper preparation. J.L. was supported partially by the National Natural Science Foundation of China through Grant No. 11675058 and by the Fundamental Research Funds for the Central Universities (Huazhong University of Science and Technology) under Project No. 2018KFYYXJJ037. C.D. was supported partially by the National Natural Science Foundation of China through Grants No. 11705131 and No. U1504111, as well as by the Science Research Funds of Wuhan Institute of Technology under Project No. K201744. Y.W. was supported partially by the National Key Research and Development Program of China under Contract No. 2016YFA0301200 as well as by the National Natural Science Foundation of China through Grants No. 11875029 and No. 11574104.

[1] H. Kimble and L. Mandel, Theory of resonance fluorescence, Phys. Rev. A **13**, 2123 (1976).
[2] H. Carmichael and D. Walls, Proposal for the measurement of the resonant Stark effect by photon correlation techniques, J. Phys. B: At. Mol. Phys. **9**, L43 (1976).
[3] H. J. Kimble, M. Dagenais, and L. Mandel, Photon Antibunching in Resonance Fluorescence, Phys. Rev. Lett. **39**, 691 (1977).
[4] J. T. Höffges, H. W. Baldauf, T. Eichler, S. R. Helmfrid, and H. Walther, Heterodyne measurement of the fluorescent radiation of a single trapped ion, Opt. Commun. **133**, 170 (1997).
[5] R. J. Glauber, *Quantum Theory of Optical Coherence: Selected Papers and Lectures* (Wiley, Weinheim, 2007).
[6] E. Knill, R. Laflamme, and G. J. Milburn, A scheme for efficient quantum computation with linear optics, Nature (London) **409**, 46 (2001).
[7] P. Kok, W. J. Munro, K. Nemoto, T. C. Ralph, J. P. Dowling, and G. J. Milburn, Linear optical quantum computing with photonic qubits, Rev. Mod. Phys. **79**, 135 (2007).
[8] H. J. Kimble, The quantum internet, Nature (London) **453**, 1023 (2008).

[9] J. L. O'Brien, A. Furusawa, and J. Vučković, Photonic quantum technologies, Nat. Photonics **3**, 687 (2009).

[10] H. J. Kimble, in *Cavity Quantum Electrodynamics*, edited by P. Berman (Academic, San Diego, 1994).

[11] H. Mabuchi and A. C. Doherty, Cavity quantum electrodynamics: Coherence in context, Science **298**, 1372 (2002).

[12] J. M. Fink, M. Göppl, M. Baur, R. Bianchetti, P. J. Leek, A. Blais, and A. Wallraff, Climbing the Jaynes-Cummings ladder and observing its $\sqrt{n}$ nonlinearity in a cavity QED system, Nature (London) **454**, 315 (2008).

[13] B. W. Shore and P. L. Knight, The Jaynes-Cummings model, J. Mod. Opt. **40**, 1195 (1993).

[14] J. Kasprzak, S. Reitzenstein, E. A. Muljarov, C. Kistner, C. Schneider, M. Strauss, S. Höling, A. Forchel, and W. Langbein, Up on the Jaynes-Cummings ladder of a quantum-dot/microcavity system, Nat. Mater. **9**, 304 (2010).

[15] F. P. Laussy, E. del Valle, M. Schrapp, A. Laucht, and J. J. Finley, Climbing the Jaynes-Cummings ladder by photon counting, J. Nanophotonics **6**, 061803 (2012).

[16] K. M. Birnbaum, A. Boca, R. Miller, A. D. Boozer, T. E. Northup, and H. J. Kimble, Photon blockade in an optical cavity with one trapped atom, Nature (London) **436**, 87 (2005).

[17] B. Dayan, A. S. Parkins, T. Aoki, E. P. Ostby, K. J. Vahala, and H. J. Kimble, A photon turnstile dynamically regulated by one atom, Science **319**, 1062 (2008).

[18] A. Faraon, I. Fushman, D. Englund, N. Stoltz, P. Petroff, and J. Vučković, Coherent generation of non-classical light on a chip via photon-induced tunneling and blockade, Nat. Phys. **4**, 859 (2008).

[19] A. Reinhard, T. Volz, M. Winger, A. Badolato, K. J. Hennessy, E. L. Hu, and A. Imamoğlu, Strongly correlated photons on a chip, Nat. Photonics **6**, 93 (2012).

[20] C. Hamsen, K. N. Tolazzi, T. Wilk, and G. Rempe, Two-Photon Blockade in an Atom-Driven Cavity QED System, Phys. Rev. Lett. **118**, 133604 (2017); M. Koch, C. Sames, M. Balbach, H. Chibani, A. Kubanek, K. Murr, T. Wilk, and G. Rempe, Three-Photon Correlations in a Strongly Driven Atom-Cavity System, *ibid.* **107**, 023601 (2011).

[21] For recent reviews, see M. Radulaski, K. Fischer, and J. Vučković, Nonclassical light generation from III-V and group-IV solid-state cavity quantum systems, Adv. At. Mol. Opt. Phys. **66**, 111 (2017); R. Trivedi, K. A. Fischer, J. Vučković, and K. Müller, Generation of non-classical light using semiconductor quantum dots, Adv. Quantum Technol. **3**, 1900007 (2020); E. Zubizarreta Casalengua, J. C. López Carreño, F. P. Laussy, and E. del Valle, Conventional and unconventional photon statistics, Laser Photonics Rev. **14**, 1900279 (2020).

[22] A. Imamoğlu, H. Schmidt, G. Woods, and M. Deutsch, Strongly Interacting Photons in a Nonlinear Cavity, Phys. Rev. Lett. **79**, 1467 (1997).

[23] Y.-X. Liu, X.-W. Xu, A. Miranowicz, and F. Nori, From blockade to transparency: Controllable photon transmission through a circuit-QED system, Phys. Rev. A **89**, 043818 (2014).

[24] A. J. Hoffman, S. J. Srinivasan, S. Schmidt, L. Spietz, J. Aumentado, H. E. Tureci, and A. A. Houck, Dispersive Photon Blockade in a Superconducting Circuit, Phys. Rev. Lett. **107**, 053602 (2011).

[25] C. Lang, D. Bozyigit, C. Eichler, L. Steffen, J. M. Fink, A. A. Abdumalikov, Jr., M. Baur, S. Filipp, M. P. da Silva, A. Blais, and A. Wallraff, Observation of Resonant Photon Blockade at Microwave Frequencies using Correlation Function Measurements, Phys. Rev. Lett. **106**, 243601 (2011).

[26] J. T. Shen and S. H. Fan, Strongly Correlated Two-Photon Transport in a One-Dimensional Waveguide Coupled to a Two-Level System, Phys. Rev. Lett. **98**, 153003 (2007); Strongly correlated multiparticle transport in one dimension through a quantum impurity, Phys. Rev. A **76**, 062709 (2007).

[27] S. Mahmoodian, M. Čepulkovskis, S. Das, P. Lodahl, K. Hammerer, and A. S. Sørensen, Strongly Correlated Photon Transport in Waveguide Quantum Electrodynamics with Weakly Coupled Emitters, Phys. Rev. Lett. **121**, 143601 (2018).

[28] M. Aspelmeyer, T. J. Kippenberg, and F. Marquardt, Cavity optomechanics, Rev. Mod. Phys. **86**, 1391 (2014).

[29] P. Rabl, Photon Blockade Effect in Optomechanical Systems, Phys. Rev. Lett. **107**, 063601 (2011).

[30] L. Neumeier, T. E. Northup, and D. E. Chang, Reaching the optomechanical strong-coupling regime with a single atom in a cavity, Phys. Rev. A **97**, 063857 (2018).

[31] D. E. Chang, V. Vuletić, and M. D. Lukin, Quantum nonlinear optics–photon by photon, Nat. Photonics **8**, 685 (2014); M. Gullans, D. E. Chang, F. H. L. Koppens, F. J. García de Abajo, and M. D. Lukin, Single-Photon Nonlinear Optics with Graphene Plasmons, Phys. Rev. Lett. **111**, 247401 (2013).

[32] R. Sáez-Blázquez, J. Feist, A. I. Fernández-Domínguez, and F. J. García-Vidal, Enhancing photon correlations through plasmonic strong coupling, Optica **4**, 1363 (2017).

[33] F. Peyskens and D. Englund, Quantum photonics model for nonclassical light generation using integrated nanoplasmonic cavity-emitter systems, Phys. Rev. A **97**, 063844 (2018).

[34] A. Majumdar, C. M. Dodson, T. K. Fryett, A. Zhan, S. Buckley, and D. Gerace, Hybrid 2D material nanophotonics: A scalable platform for low-power nonlinear and quantum optics, ACS Photon. **2**, 1160 (2015); A. Majumdar and D. Gerace, Single-photon blockade in doubly resonant nanocavities with second-order nonlinearity, Phys. Rev. B **87**, 235319 (2013).

[35] A. Ryou, D. Rosser, A. Saxena, T. Fryett, and A. Majumdar, Strong photon antibunching in weakly nonlinear two-dimensional exciton-polaritons, Phys. Rev. B **97**, 235307 (2018).

[36] A. Ridolfo, M. Leib, S. Savasta, and M. J. Hartmann, Photon Blockade in the Ultrastrong Coupling Regime, Phys. Rev. Lett. **109**, 193602 (2012); A. Ridolfo, S. Savasta, and M. J. Hartmann, Nonclassical Radiation from Thermal Cavities in the Ultrastrong Coupling Regime, *ibid.* **110**, 163601 (2013).

[37] A. Miranowicz, M. Paprzycka, Y.-x. Liu, J. Bajer, and F. Nori, Two-photon and three-photon blockades in driven nonlinear systems, Phys. Rev. A **87**, 023809 (2013).

[38] J. Restrepo, I. Favero, and C. Ciuti, Fully coupled hybrid cavity optomechanics: Quantum interferences and correlations, Phys. Rev. A **95**, 023832 (2017).

[39] C. J. Zhu, Y. P. Yang, and G. S. Agarwal, Collective multiphoton blockade in cavity quantum electrodynamics, Phys. Rev. A **95**, 063842 (2017).

[40] R. Huang, A. Miranowicz, J.-Q. Liao, F. Nori, and H. Jing, Nonreciprocal Photon Blockade, Phys. Rev. Lett. **121**, 153601 (2018).

[41] D. S. Wild, E. Shahmoon, S. F. Yelin, and M. D. Lukin, Quantum Nonlinear Optics in Atomically Thin Materials, Phys. Rev. Lett. **121**, 123606 (2018).

[42] T. C. H. Liew and V. Savona, Single Photons from Coupled Quantum Modes, Phys. Rev. Lett. **104**, 183601 (2010).

[43] M. Bamba, A. Imamoğlu, I. Carusotto, and C. Ciuti, Origin of strong photon antibunching in weakly nonlinear photonic molecules, Phys. Rev. A **83**, 021802(R) (2011).

[44] H. Flayac and V. Savona, Input-output theory of the unconventional photon blockade, Phys. Rev. A **88**, 033836 (2013).

[45] S. Ferretti, V. Savona, and D. Gerace, Optimal antibunching in passive photonic devices based on coupled nonlinear resonators, New J. Phys. **15**, 025012 (2013).

[46] D. Gerace and V. Savona, Unconventional photon blockade in doubly resonant microcavities with second-order nonlinearity, Phys. Rev. A **89**, 031803(R) (2014).

[47] For a recent review see H. Flayac and V. Savona, Unconventional photon blockade, Phys. Rev. A **96**, 053810 (2017); H. Flayac, D. Gerace, and V. Savona, An all-silicon single-photon source by unconventional photon blockade, Sci. Rep. **5**, 11223 (2015).

[48] X.-W. Xu and Y. Li, Tunable photon statistics in weakly nonlinear photonic molecules, Phys. Rev. A **90**, 043822 (2014).

[49] H. Z. Shen, Y. H. Zhou, and X. X. Yi, Tunable photon blockade in coupled semiconductor cavities, Phys. Rev. A **91**, 063808 (2015).

[50] H. Flayac and V. Savona, Single photons from dissipation in coupled cavities, Phys. Rev. A **94**, 013815 (2016).

[51] A. Majumdar, M. Bajcsy, A. Rundquist, and J. Vučković, Loss-Enabled Sub-Poissonian Light Generation in a Bimodal Nanocavity, Phys. Rev. Lett. **108**, 183601 (2012).

[52] W. Zhang, Z. Y. Yu, Y. M. Liu, and Y. W. Peng, Optimal photon antibunching in a quantum-dot-bimodal-cavity system, Phys. Rev. A **89**, 043832 (2014).

[53] J. Li and Y. Wu, Quality of photon antibunching in two cavity-waveguide arrangements on a chip, Phys. Rev. A **98**, 053801 (2018).

[54] Y. L. Liu, G. Z. Wang, Y.-X. Liu, and F. Nori, Mode coupling and photon antibunching in a bimodal cavity containing a dipole quantum emitter, Phys. Rev. A **93**, 013856 (2016).

[55] X. W. Xu and Y. J. Li, Antibunching photons in a cavity coupled to an optomechanical system, J. Phys. B: At., Mol. Opt. Phys. **46**, 035502 (2013).

[56] V. Savona, Unconventional photon blockade in coupled optomechanical systems, arXiv:1302.5937; B. Sarma and A. K. Sarma, Unconventional photon blockade in three-mode optomechanics, Phys. Rev. A **98**, 013826 (2018).

[57] A. Miranowicz, J. Bajer, N. Lambert, Y.-x. Liu, and F. Nori, Tunable multiphonon blockade in coupled nanomechanical resonators, Phys. Rev. A **93**, 013808 (2016).

[58] M. Bamba and C. Ciuti, Counter-polarized single-photon generation from the auxiliary cavity of a weakly nonlinear photonic molecule, Appl. Phys. Lett. **99**, 171111 (2011).

[59] O. Kyriienko, I. A. Shelykh, and T. C. H. Liew, Tunable single-photon emission from dipolaritons, Phys. Rev. A **90**, 033807 (2014).

[60] J. C. López Carreño, C. Sánchez Muñoz, D. Sanvitto, E. del Valle, and F. P. Laussy, Exciting Polaritons with Quantum Light, Phys. Rev. Lett. **115**, 196402 (2015).

[61] J. C. López Carreño and F. P. Laussy, Excitation with quantum light. I. Exciting a harmonic oscillator, Phys. Rev. A **94**, 063825 (2016); J. C. López Carreño, C. Sánchez Muñoz, E. del Valle, and F. P. Laussy, Excitation with quantum light. II. Exciting a two-level system, *ibid.* **94**, 063826 (2016).

[62] C. W. Gardiner, Driving a Quantum System with the Output Field from another Driven Quantum System, Phys. Rev. Lett. **70**, 2269 (1993).

[63] H. J. Carmichael, Quantum Trajectory Theory for Cascaded Open Systems, Phys. Rev. Lett. **70**, 2273 (1993).

[64] C. Gardiner and P. Zoller, *Quantum Noise: A Handbook of Markovian and Non-Markovian Quantum Stochastic Methods with Applications to Quantum Optics* (Springer, Berlin, 2004).

[65] S. C. Azizabadi, N. L. Naumann, M. Katzer, A. Knorr, and A. Carmele, Quantum cascade driving: Dissipatively mediated coherences, Phys. Rev. A **96**, 023816 (2017).

[66] P. Kurpiers, P. Magnard, T. Walter, B. Royer, M. Pechal, J. Heinsoo, Y. Salath, A. Akin, S. Storz, J.-C. Besse *et al.*, Deterministic quantum state transfer and remote entanglement using microwave photons, Nature (London) **558**, 264 (2018).

[67] Y. F. Xiao, V. Gaddam, and L. Yang, Coupled optical microcavities: An enhanced refractometric sensing configuration, Opt. Express **16**, 12538 (2008).

[68] Y. F. Xiao, M. Li, Y. C. Liu, Y. Li, X. Sun, and Q. Gong, Asymmetric Fano resonance analysis in indirectly coupled microresonators, Phys. Rev. A **82**, 065804 (2010).

[69] J. Pan, S. Sandhu, Y. Huo, M. Povinelli, J. S. Harris, M. M. Fejer, and S. Fan, Experimental demonstration of an all-optical analog to the superradiance effect in an on-chip photonic crystal resonator system, Phys. Rev. B **81**, 041101 (2010).

[70] H. Pichler and P. Zoller, Photonic Circuits with Time Delays and Quantum Feedback, Phys. Rev. Lett. **116**, 093601 (2016).

[71] R. Loudon, *The Quantum Theory of Light* (Oxford University, Oxford, 2003).

[72] Y. Akahane, T. Asano, B. S. Song, and S. Noda, High-Q photonic nanocavity in a two-dimensional photonic crystal, Nature (London) **425**, 944 (2003).

[73] M. Notomi, E. Kuramochi, and T. Tanabe, Large-scale arrays of ultrahigh-Q coupled nanocavities, Nat. Photonics **2**, 741 (2008).

[74] M. F. Yanik, W. Suh, Z. Wang, and S. Fan, Stopping Light in a Waveguide with an All-Optical Analog of Electromagnetically Induced Transparency, Phys. Rev. Lett. **93**, 233903 (2004).

[75] X. Yang, M. Yu, D. L. Kwong, and C. W. Wong, All-Optical Analog to Electromagnetically Induced Transparency in Multiple Coupled Photonic Crystal Cavities, Phys. Rev. Lett. **102**, 173902 (2009).

[76] X. Yang, M. Yu, D. L. Kwong, and C. W. Wong, Coupled resonances in multiple silicon photonic crystal cavities in all-optical solid-state analogy to electromagnetically induced transparency, IEEE J. Sel. Top. Quantum Electron. **16**, 288 (2010).

[77] J. R. Petta, A. C. Johnson, J. M. Taylor, E. A. Laird, A. Yacoby, M. D. Lukin, C. M. Marcus, M. P. Hanson, and A. C. Gossard, Coherent manipulation of coupled electron spins in semiconductor quantum dots, Science **309**, 2180 (2005).

[78] M. Atatüre, J. Dreiser, A. Badolato, A. Högele, K. Karrai, and A. Imamoglu, Quantum-dot spin-state preparation with near-unity fidelity, Science **312**, 551 (2006).

[79] B. Alloing, C. Zinoni, V. Zwiller, L. H. Li, C. Monat, M. Gobet, G. Buchs, A. Fiore, E. Pelucchi, and E. Kapon, Growth and

characterization of single quantum dots emitting at 1300 nm, Appl. Phys. Lett. **86**, 101908 (2005).

[80] T. Kojima, K. Kojima, T. Asano, and S. Noda, Accurate alignment of a photonic crystal nanocavity with an embedded quantum dot based on optical microscopic photoluminescence imaging, Appl. Phys. Lett. **102**, 011110 (2013).

[81] T. Yoshie, A. Scherer, J. Hendrickson, G. Khitrova, H. M. Gibbs, G. Rupper, C. Ell, O. B. Shchekin, and D. G. Deppe, Vacuum Rabi splitting with a single quantum dot in a photonic crystal nanocavity, Nature (London) **432**, 200 (2004).

[82] J. Vučković, Quantum optics and cavity QED with quantum dots in photonic crystals, in *Quantum Optics and Nanophotonics*, edited by C. Fabre, V. Sandoghdar, N. Treps, and L. F. Cugliandolo (Oxford University Press, Oxford, 2017), pp. 365–406.

[83] A. Faraon, D. Englund, I. Fushman, J. Vučković, N. Stoltz, and P. Petroff, Local quantum dot tuning on photonic crystal chips, Appl. Phys. Lett. **90**, 213110 (2007).

[84] D. Englund, A. Faraon, I. Fushman, N. Stoltz, P. Petroff, and J. Vučković, Controlling cavity reflectivity with a single quantum dot, Nature (London) **450**, 857 (2007).

[85] A. Majumdar, A. Rundquist, M. Bajcsy, and J. Vučković, Cavity quantum electrodynamics with a single quantum dot coupled to a photonic molecule, Phys. Rev. B **86**, 045315 (2012).

[86] I. Fushman, D. Englund, A. Faraon, N. Stoltz, P. Petroff, and J. Vučković, Controlled phase shifts with a single quantum dot, Science **320**, 769 (2008).

[87] H. Kim, T. C. Shen, K. Roy-Choudhury, G. S. Solomon, and E. Waks, Resonant Interactions between a Mollow Triplet Sideband and a Strongly Coupled Cavity, Phys. Rev. Lett. **113**, 027403 (2014).

[88] D. Englund, A. Majumdar, A. Faraon, M. Toishi, N. Stoltz, P. Petroff, and J. Vučković, Resonant Excitation of a Quantum Dot Strongly Coupled to a Photonic Crystal Nanocavity, Phys. Rev. Lett. **104**, 073904 (2010).

[89] D. Englund, I. Fushman, A. Faraon, and J. Vučković, Quantum dots in photonic crystals: From quantum information processing to single photon nonlinear optics, Photonics Nanostruct. **7**, 56 (2009).

[90] I. Favero, A. Berthelot, G. Cassabois, C. Voisin, C. Delalande, P. Roussignol, R. Ferreira, and J. M. Gérard, Temperature dependence of the zero-phonon linewidth in quantum dots: An effect of the fluctuating environment, Phys. Rev. B **75**, 073308 (2007).

[91] D. Takamiya, Y. Ota, R. Ohta, H. Takagi, N. Kumagai, S. Ishida, S. Iwamoto, and Y. Arakawa, in *Proceedings of the 2013 Conference on Lasers and Electro-Optics Pacific Rim, Kyoto, Japan* (Optical Society of America, 2013), paper MI2_2.

[92] Y. Ota, S. Iwamoto, N. Kumagai, and Y. Arakawa, Spontaneous Two-Photon Emission from a Single Quantum Dot, Phys. Rev. Lett. **107**, 233602 (2011).

[93] A. de Rossi, M. Lauritano, S. Combrié, Q. V. Tran, and C. Husko, Interplay of plasma-induced and fast thermal nonlinearities in a GaAs-based photonic crystal nanocavity, Phys. Rev. A **79**, 043818 (2009).

[94] R. Hanbury Brown and R. Q. Twiss, Correlation between photons in two coherent beams of light, Nature (London) **177**, 27 (1956).

[95] K. Müller, A. Rundquist, K. A. Fischer, T. Sarmiento, K. G. Lagoudakis, Y. A. Kelaita, C. S. Muñoz, E. del Valle, F. P. Laussy, and J. Vučković, Coherent Generation of Nonclassical Light on Chip via Detuned Photon Blockade, Phys. Rev. Lett. **114**, 233601 (2015).